JACS Au
AN OPEN ACCESS JOURNAL OF THE AMERICAN CHEMICAL SOCIETY

pubs.acs.org/jacsau

Article

Strain-Negligible Eu^{2+} Doping Enabled Color-Tunable Harsh Condition-Resistant Perovskite Nanocrystals for Superior Light-Emitting Diodes

Mengdie Jin, Zhichao Zeng, Hao Fu, Siyuan Wang, Zongyou Yin,* Xinyun Zhai, Qian Zhang, and Yaping Du*

Cite This: *JACS Au* 2023, 3, 216–226

Read Online

ACCESS | Metrics & More | Article Recommendations | Supporting Information

ABSTRACT: Cesium lead halide ($CsPbX_3$, X = Br, Cl, I) perovskite nanocrystals (NCs) possess tunable band gaps across the entire visible spectral range and are promising for various optoelectronic device applications. However, poor performance in adverse conditions limits their further development in practical optoelectronics. Herein, highly stable perovskite NCs are developed by doping europium(II) (Eu^{2+}) into the B-site of $CsPbBr_3$ with negligible lattice distortion/strain. Eu^{2+}-doped $CsPbBr_3$ NCs exhibit tunable green-to-cyan emissions, high photoluminescence quantum yield, and good resistance to harsh conditions, including ultraviolet irradiation, erosion of moisture, and corrosion of polar solvent molecules. In particular, the thermal stability of $CsPbBr_3$ NCs after Eu^{2+} doping is greatly enhanced under continuous heating in air, while exhibiting the emissions of Eu^{2+}. Furthermore, a Eu^{2+}-doped $CsPbBr_3$ NC-based cyan light-emitting diode is fabricated, which exhibits narrow exciton emission driven under different current densities. This work would open the avenue to develop the rational lanthanide ion doping strategy for further advancing perovskite nanomaterials toward practical applications.

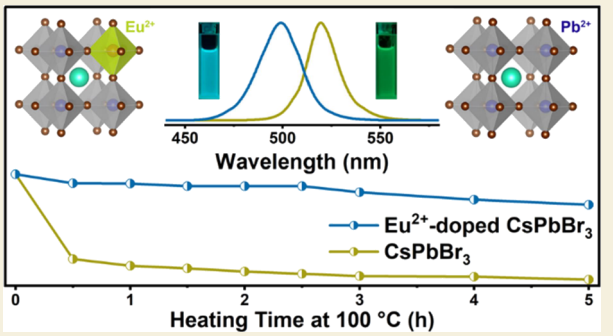

KEYWORDS: *$CsPbBr_3$ perovskite nanocrystals, lanthanide, adjustable luminescence, stability*

1. INTRODUCTION

Since the first report in 2015, cesium lead halide ($CsPbX_3$, X = Br, Cl, I) nanocrystals (NCs) demonstrate excellent photophysical properties including low cost, strong excitonic absorption, high photoluminescence quantum yield (PLQY), narrow excitonic emission spectra, and tunable luminescence achieved by changing the halogen composition.[1,2] Hence, $CsPbX_3$ perovskite has been widely applied in light-emitting diodes (LEDs),[1,3−8] solar cells,[9−12] lasers,[13] scintillators,[14,15] and optoelectronic devices in recent years.[16] As typical all-inorganic halide perovskite, $CsPbBr_3$, which can be synthesized through many methods,[14,16−21] exhibits efficient bright monochrome green narrow emission and attracts wide attention in many fields. However, $CsPbBr_3$ NCs also suffer from two critical issues, which are lead (Pb) toxicity and poor moisture/heat resistance. In order to address these challenges, B-site doping with lanthanide (Ln) ions or transition metal ions has so far been recognized as a promising solution to regulate the electronic structure and optical properties of halide perovskite NCs, while reducing the toxicity of lead.[22−25]

Ln ions have abundant 4f energy levels and unique electron configurations.[26] Ln ions, as optically active centers, provide energy levels within the band gap of the material and produce optical transitions at frequencies below the fundamental absorption, thus endowing the host with interesting optical properties.[23] The transitions of 4f → 4f or 5d → 4f inside Ln ions increase the luminescence intensity and color purity of $CsPbX_3$ NCs.[27] According to the Goldschmidt tolerance factor (t) and the octahedral factor (μ), the electronic structure and optical properties of halide perovskite can be adjusted by selecting suitable Ln ions to replace the B-site divalent metal ions. For example, Yu and co-workers have improved the quantum yield of $CsPbBr_3$ NCs up to 89% by doping cerium(III) (Ce^{3+}), a factor of 2 increase compared to the undoped ones. Zhang and co-workers have reported that $CsPbBr_3$ NCs doped with neodymium(III) (Nd^{3+}) realized highly efficient blue emission, the PLQYs of which reached 90%, achieving efficient LED devices.[28] Liu and co-workers have reported that europium(III) (Eu^{3+})-doped $CsPbBr_xCl_{3-x}$

Received: October 31, 2022
Revised: November 21, 2022
Accepted: November 23, 2022
Published: December 21, 2022

https://doi.org/10.1021/jacsau.2c00593
JACS Au 2023, 3, 216–226

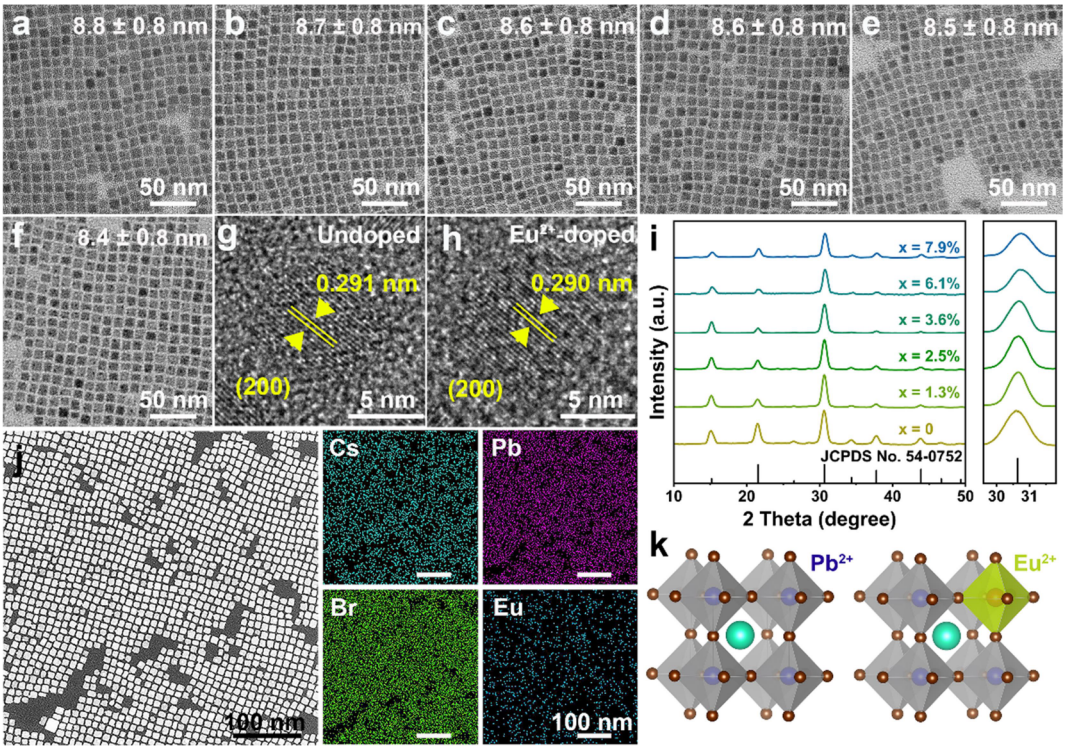

Figure 1. (a–f) TEM images of Eu^{2+}-doped $CsPbBr_3$ NCs with a Eu^{2+} doping ratio of x = 0%, x = 1.3%, x = 2.5%, x = 3.6%, x = 6.1%, x = 7.9%. (g,h) HRTEM images of undoped and Eu^{2+}-doped $CsPbBr_3$ (x = 7.9%) NCs. (i) XRD patterns of all Eu^{2+}-doped $CsPbBr_3$ NCs. (j) STEM image and elemental mappings of Cs, Pb, Eu, and Br elements in the Eu^{2+}-doped $CsPbBr_3$ (x = 7.9%) NCs. (k) Schematic illustration showing that Eu^{2+} replaces Pb^{2+}.

NCs had exciton emission and red emission of Eu^{3+}, attributed to the energy transfer from excitons to dopants, which was featured with temperature dependence.[29] However, in the previous studies, the valence state of Ln^{3+}, doped into $CsPbBr_3$ NCs, is inconsistent with that of Pb^{2+}, and their ionic radius is quite different.[25,27−29] Moreover, a significant improvement in terms of stability caused by doping Ln^{3+} into $CsPbBr_3$ NCs has not been reported.

The incorporation of divalent transition metal elements into $CsPbX_3$ has been proved to effectively eliminate the inherent defects of crystals.[30,31] Sun and co-workers have eliminated inherent defects such as halide vacancies by doping nickel(II) (Ni^{2+}) into $CsPbCl_3$ NCs, resulting in increasing the short-range order of the lattice and improving the QY of violet light.[31] Wang et al. have reported that the anion exchange reaction of copper(II) Cu^{2+}-assisted $CsPbCl/Br_3$ NCs resulted in a well-defined crystal structure with fewer surface defects and higher optical stability at room temperature.[30] Typically, the ionic radii of divalent transition metals (Ni^{2+} 69, Cu^{2+} 73 ppm) are too different from those of lead ions, resulting in non-negligible deformation/strain in the crystal structure owing to doping. However, there are few reports on improving the stability in harsh conditions by doping $CsPbBr_3$ NCs with divalent ions.

When the dopant ions are selectively incorporated into $CsPbBr_3$ NCs, the size and valence of the doped ions should be close to those of the host cations to reduce doping-induced lattice defects.[32] Among the Ln, Eu, which exists in either the divalent or trivalent ion valence state, is an effective sensitizer for PL of perovskite materials[29,33] and also plays a crucial role in improving the thermal stability of perovskite materials.[34−36] Theoretical studies have reported that Eu^{2+} can successfully substitute Pb^{2+} sites due to the comparable ionic size under the fact that Eu^{2+} (117 pm) is very close to that of Pb^{2+} (119 pm). Therefore, the doping of Eu^{2+} into the host of $CsPbBr_3$ NCs may result in negligible distortion/strain in crystal structures, benefiting energetic stability of the system.[37] Thence, this inspires us to employ Eu^{2+} as the B-site dopant to explore the optical performance and stability of $CsPbBr_3$ NCs in conventional environments, even in specific harsh conditions.

In this work, highly stable and cyan-emitting perovskite NCs were synthesized by doping the B-site of $CsPbBr_3$ with the Ln ion Eu^{2+}. With the increase of the Eu^{2+} doping ratio (x = Eu^{2+}/(Eu^{2+} + Pb^{2+})), the narrow band singlet emission of Eu^{2+}-doped $CsPbBr_3$ NCs can be fine-tuned from green to cyan with full width at half maximum (FWHM) of the emission peaks less than 30 nm. Upon different Eu^{2+} doping, the PLQY values range from 55 to 90%, and radiative lifetimes range from 4.55 to 26.45 ns. Meanwhile, the incorporation of Eu^{2+} slightly decreases the band gap of $CsPbBr_3$ without changing the crystal structure. Importantly, Eu^{2+} doping significantly improves the stability of $CsPbBr_3$ NCs to withstand various harsh conditions, including ultraviolet (UV) irradiation, erosion of water and polar solvent molecules, and thermal effect on luminescence intensity up to 100 °C in air. Under specific heating temperatures, the emission of Eu^{2+}-doped $CsPbBr_3$ NCs under UV excitation changes from cyan to blue light, indicating that Eu^{2+}-doped $CsPbBr_3$ NCs not only exhibit exciton emission but also Eu^{2+} emission, and the intensity ratio of the two peaks is variable. Based on the improved stability and QY, a Eu^{2+}-doped $CsPbBr_3$ (x = 7.9%) NCs-based cyan LED is prepared, showing narrow emission under different current densities. This work indicates that Ln(II) ion B-site

https://doi.org/10.1021/jacsau.2c00593
JACS Au 2023, 3, 216−226

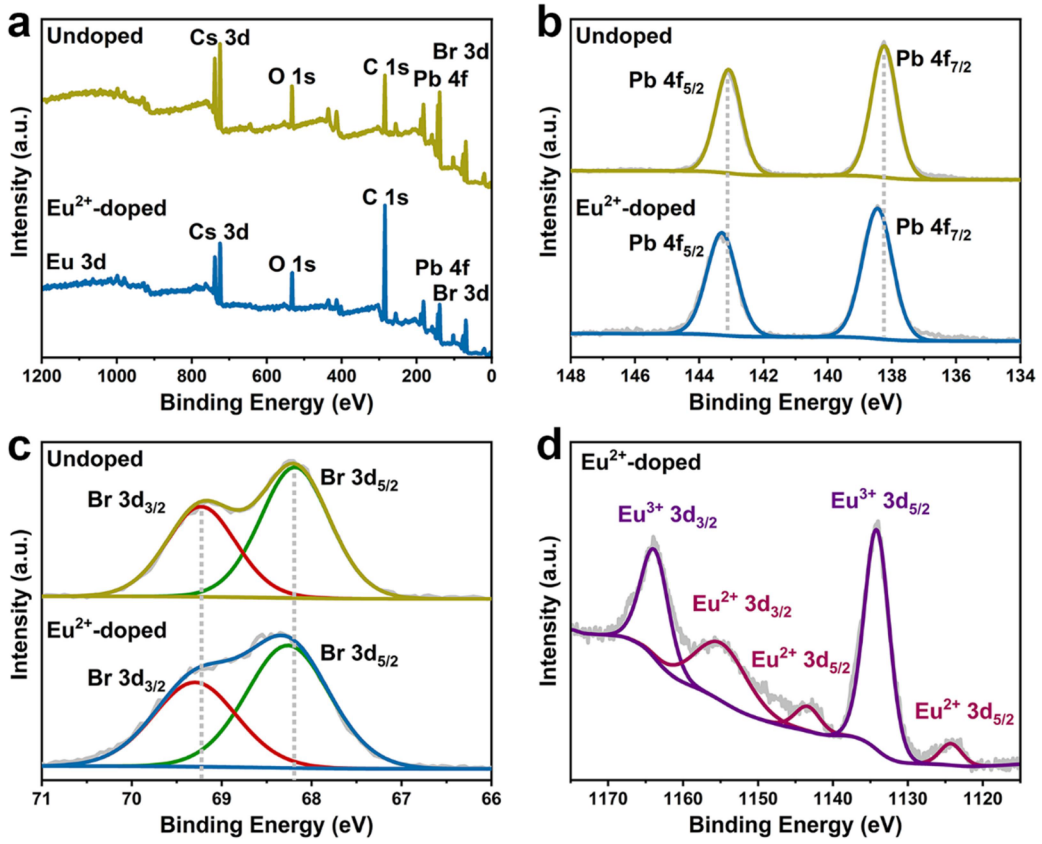

Figure 2. (a) XPS spectra of undoped and Eu^{2+}-doped $CsPbBr_3$ (x = 7.9%) NCs. High-resolution XPS spectra corresponding to (b) Pb 4f, (c) Br 3d, and (d) Eu 3d.

doping is a reliable strategy to make perovskites more robust for broader optoelectronic applications.

2. RESULTS AND DISCUSSION

Referring to a previous work, Eu^{2+}-doped $CsPbBr_3$ NCs with different Eu^{2+} doping ratios are successfully synthesized by the hot-injection colloid chemistry method. In order to prevent the occurrence of Eu^{3+} caused by rapid oxidization of Eu^{2+} in air, the solvent should be purified to remove water, and the precursor should be kept in an oxygen-free and water-free state before synthesis. First of all, it is necessary to eliminate the influence associated with the quantum confinement effect caused by different particle morphologies or sizes, in order to quantitatively compare the influence of Eu^{2+}-doping on $CsPbBr_3$ NCs. Morphologies and structures of Eu^{2+}-doped $CsPbBr_3$ NCs with different Eu^{2+} doping ratios are characterized by transmission electron microscopy (TEM). As shown in Figure 1a–f, the TEM images of both undoped and Eu^{2+}-doped $CsPbBr_3$ NCs with different Eu^{2+} doping ratios show cubelike morphologies with no obvious change in terms of sizes (around 8 nm) and morphologies (Figure S1). During the measurement, prolonged exposure of $CsPbBr_3$ NCs to high-energy incident electron beams resulted in the appearance of black spots in the TEM images, which could be reasonably explained by the reduction of Pb^{2+} ions to metallic Pb^0.[38] As the high-resolution TEM (HRTEM) images shown in Figure 1g,h, the interplanar distances of the (200) plane of undoped and Eu^{2+}-doped $CsPbBr_3$ (x = 7.9%) NCs are determined to be 0.291 and 0.290 nm, respectively. Because of the replacement of Pb^{2+} by Eu^{2+} with a smaller ion radius, the lattice contraction of $CsPbBr_3$ NCs form smaller plane spacing. Doped Eu^{2+} has a limited effect on lattice contraction, which is similar to the predicted results of theoretical calculations as previously reported.[37] As X-ray diffraction (XRD) patterns show in Figure 1i, all NCs have similar diffraction peaks patterns, indicating that the perovskite phases (Joint Committee on Powder Diffraction Standards (JCPDS) Portable Document Format (PDF) #54-0752) formed undoped and Eu^{2+}-doped $CsPbBr_3$ NCs with different Eu^{2+} doping ratios. The diffraction peaks shift to a higher angle as the Eu^{2+} doping ratio increases, confirming that the lattice slightly shrinks. The scanning TEM (STEM) image shown in Figure 1j demonstrates the uniform cubic morphologies of Eu^{2+}-doped $CsPbBr_3$ (x = 7.9%) NCs. The corresponding energy dispersive X-ray spectroscopy (EDS) mapping images shows the existence of Pb, Br, and Eu elements, indicating that Eu^{2+} has been incorporated into $CsPbBr_3$ NCs (Figure S2). The quantitative Eu^{2+} doping ratios of Eu^{2+}-doped $CsPbBr_3$ NCs are measured by inductively coupled plasma optical emission spectrometry (ICP-OES, Table S1), which also confirms that Eu^{2+} is successfully doped into $CsPbBr_3$ NCs, replacing the Pb^{2+} site, as shown in Figure 1j.

X-ray photoelectron spectroscopy (XPS) measurements of undoped and Eu^{2+}-doped $CsPbBr_3$ (x = 7.9%) NCs are performed to verify whether Eu^{2+} was successfully doped into $CsPbBr_3$ NCs and replaced Pb^{2+} to achieve B-site doping. As the XPS survey spectra show in Figure 2a, both undoped and Eu^{2+}-doped (x = 7.9%) NCs comprise Cs, Pb, Br, C, and O elements. For Eu^{2+}-doped $CsPbBr_3$ NCs, the Pb^{2+} $4f_{5/2}$ and Pb^{2+} $4f_{7/2}$ peaks and the Br^- $3d_{3/2}$ and $3d_{5/2}$ peaks shift slightly to a higher binding energy (Figure 2b,c). However, this trend

https://doi.org/10.1021/jacsau.2c00593
JACS Au 2023, 3, 216–226

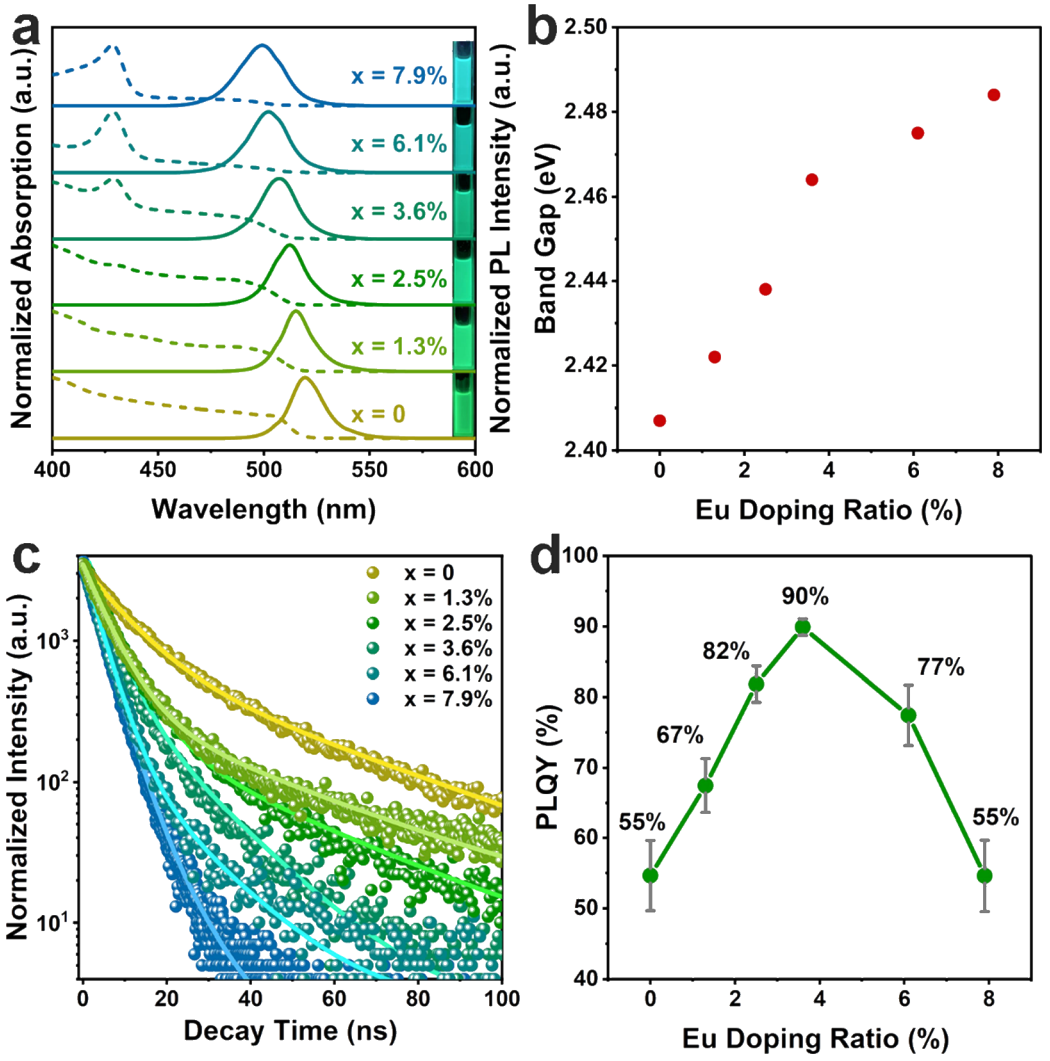

Figure 3. (a) Normalized PL and absorption spectra of Eu^{2+}-doped $CsPbBr_3$ NC solutions with a Eu^{2+} doping ratio of x = 0%, x = 1.3%, x = 2.5%, x = 3.6%, x = 6.1%, x = 7.9%: PL emission (solid line, excitation at 365 nm) and UV−vis absorbance spectra (dashed line). Inset photograph shows the corresponding images of luminescent Eu^{2+}-doped $CsPbBr_3$ NC colloidal solutions under UV excitation. (b) Band gaps of Eu^{2+}-doped $CsPbBr_3$ NCs. (c) PL decay curves of the Eu^{2+}-doped $CsPbBr_3$ NCs solutions. (d) Average PLQYs of Eu^{2+}-doped $CsPbBr_3$ NCs solutions (excitation at 365 nm).

is not observed in the Cs^+ $3d_{3/2}$ and $3d_{5/2}$ peaks (Figure S3), which indicates that the lattice shrinkage caused by Eu^{2+} doping leads to stronger Pb−Br interactions. Similar shifts in the binding energies of Pb^{2+} and Br^- are also observed in reported Nd^{3+}-doped $CsPbBr_3$ NCs.[28] Simultaneously, several peaks of Eu^{2+}-doped $CsPbBr_3$ NCs located between 1120 and 1170 eV are attributed to the Eu 3d signals of Eu^{2+} and Eu^{3+} (Figure 2d),[39] while the signals of Eu 3d are not found in undoped $CsPbBr_3$ NCs (Figure S4). Because XPS is sensitive to the surface of the tested samples, Eu^{2+} of the surface layers is highly reactive without the protection of reducing agents, resulting in the tested sample containing mixed-valence Eu.[40−42] Eu^{2+} on the surface layers of the sample exposed to air have been oxidized to Eu^{3+}, leading to the detection of $3d_{5/2}$ and $3d_{3/2}$ peaks of Eu^{3+}. The PL spectra (Figure S5) and the excitation-emission matrix of Eu^{2+}-doped $CsPbBr_3$ NCs (Figure S6) show the absence of red emission in the 590−700 nm range, which is intrinsic Eu^{3+} ion $^5D_0 \rightarrow {}^7F_J$ (J = 0−4). It further indicates that the Eu^{3+} measured by XPS is on the surface layer because of the oxidation in air, while the Eu^{2+} is in the bulk phase, and a suitable ligand is not provided in the system of $CsPbBr_3$ to enable the emission of Eu^{3+}. Based on the above analysis, Eu^{2+} successfully enters the lattice of the $CsPbBr_3$ perovskite host and takes over a fraction of the Pb^{2+} sites rather than the Cs^+ and Br^- sites.

With the intention of exploring the influence of Eu^{2+} doping on the optical properties of $CsPbBr_3$ NCs, the normalized PL and ultraviolet−visible (UV−vis) absorbance spectra of Eu^{2+}-doped $CsPbBr_3$ NCs solutions with different Eu^{2+} doping ratios are obtained, as shown in Figure 3a. With the increase in the Eu^{2+}doping ratio, both the absorption onset and the PL emission peak present a continuous blue shift, which is similar to the theoretically predicted results.[37] The inserted photographs in Figure 3a show that the colloidal solutions formed by Eu^{2+}-doped $CsPbBr_3$ NCs dispersed in toluene exhibit a transition of PL emission from green to cyan with the increased doping ratio of Eu^{2+} under UV irradiation (365 nm). Optical band gaps are quantified from the Tauc plot of $(\alpha h\nu)^2$ versus $h\nu$,[43] which illustrates the band gaps of Eu^{2+}-doped $CsPbBr_3$ NCs with different Eu^{2+} doping ratios (Figure S7). As shown in Figure 3b, the band gap of undoped $CsPbBr_3$ NCs is 2.408 eV and that of Eu^{2+}-doped $CsPbBr_3$ NCs broadens with

https://doi.org/10.1021/jacsau.2c00593
JACS Au 2023, 3, 216−226

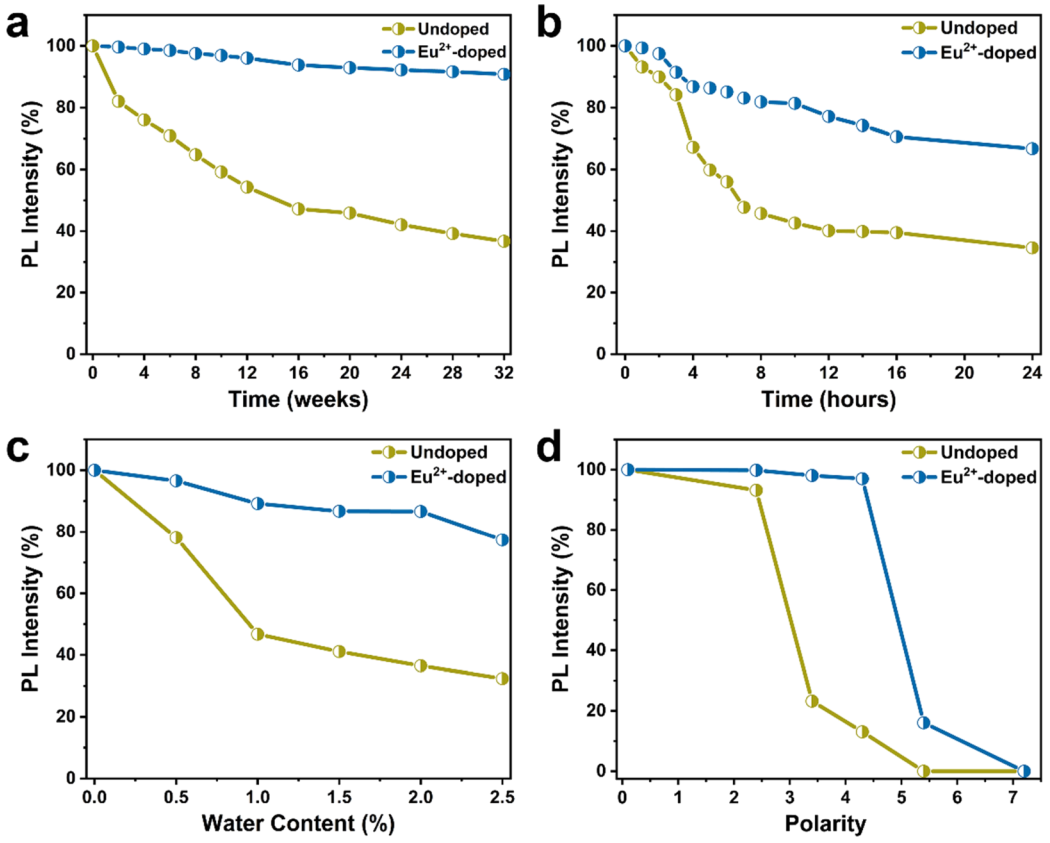

Figure 4. (a) Normalized exciton emission intensity of undoped and Eu^{2+}-doped $CsPbBr_3$ (x = 7.9%) NCs as a function of stored time in conventional environments. (b) Normalized exciton emission intensity of undoped and Eu^{2+}-doped $CsPbBr_3$ (x = 7.9%) NCs as a function of UV-irradiated time. (c) Normalized exciton emission intensity of undoped and Eu^{2+}-doped (x = 7.9%) $CsPbBr_3$ NCs as a function of the water content in the solvent. (d) Normalized exciton emission intensity of undoped and Eu^{2+}-doped (x = 7.9%) $CsPbBr_3$ NCs as a function of polarity of the dispersion solvent.

the increase of the Eu^{2+} doping ratio, corresponding to the blue shift of the PL and absorption spectra. As illustrated in Figure 3c, the PL decay curves of Eu^{2+}-doped $CsPbBr_3$ NCs colloidal solutions are fitted by a biexponential decay model (Table S2). Specifically, as the Eu^{2+} doping ratio increases from 0 to 7.9%, the average lifetime (τ_{ave}) decreases from 26.45 to 4.55 ns. On the other hand, as the Eu^{2+} doping ratio increases, the PLQY first increases from 55% of undoped $CsPbBr_3$ NCs to 90% of Eu^{2+}-doped $CsPbBr_3$ (x = 3.6%) NCs and then decreases back to 55% of Eu^{2+}-doped $CsPbBr_3$ (x = 7.9%) NCs (Figure 3d). It indicates that there exists a relatively narrow window for the incorporation amount of Eu^{2+} in $CsPbBr_3$ NCs so as to achieve a high PLQY of $CsPbBr_3$ NCs.

The PL intensity of toluene dispersion of the undoped and Eu^{2+}-doped $CsPbBr_3$ (x = 7.9%) NCs stored in conventional environments is tested (Figure 4a) with a view to investigate whether Eu^{2+} doping can improve the stability of $CsPbBr_3$ NCs. After 32 weeks, the PL intensity of Eu^{2+}-doped $CsPbBr_3$ NCs remains at 90% of the initial one, but that of undoped $CsPbBr_3$ NCs decreases to 40% of the initial one. In order to further compare the PL stability under UV irradiation, undoped and Eu^{2+}-doped $CsPbBr_3$ (x = 7.9%) NC solutions are placed under UV lamps (8 W, 365 nm) for up to 24 h at room temperature. The contamination of the sample by other lights during this period was avoided. As shown in Figure 4b, when the UV irradiation time reaches 4 h, there is a significant gap in the PL intensity between undoped and Eu^{2+}-doped $CsPbBr_3$ (x = 7.9%) NCs. When the UV irradiation time reaches 8 h, the PL intensity of the Eu^{2+}-doped NCs remains 82% of the initial value, but that of undoped NCs decreases to only 45% of the initial intensity. These results show that the introduction of Eu^{2+} significantly improves the PL stability of $CsPbBr_3$ NCs. In order to evaluate the luminescence stability in water, the undoped and Eu^{2+}-doped $CsPbBr_3$ (x = 7.9%) NCs are dispersed in ethyl acetate solutions containing different contents of water at room temperature and in the air environment, and then, the dispersions are mixed for 10 min to ensure complete invasion of water molecules. Similarly, the Eu^{2+}-doped $CsPbBr_3$ NCs are more stable than the undoped ones. As shown in Figure 4c, with the water content increase in the dispersion solvent, the PL intensity of undoped NCs is quenched sharply by water, while the PL intensity of Eu^{2+}-doped NCs decreases relatively slowly. Furthermore, undoped and Eu^{2+}-doped $CsPbBr_3$ NCs are dispersed in several solvents with different polarities (Table S3) and maintained for 10 min. Then, their PL intensities are measured for exploring tolerance to the damage from polar solvents. As shown in Figure 4d, when undoped and Eu^{2+}-doped $CsPbBr_3$ NCs are dispersed in a solvent with low polarity, such as cyclohexane or toluene, the PL intensity of the two samples is relatively high. When the polarity of the dispersion solution is medium, such as dichloromethane and ethyl acetate, the PL intensity of undoped NCs dispersed therein is reduced significantly, but that of the Eu^{2+}-doped NCs remains relatively high. When dispersed in acetone, the undoped NCs lose their luminescence, while the Eu^{2+}-doped NCs still emit cyan light.

https://doi.org/10.1021/jacsau.2c00593
JACS Au 2023, 3, 216−226

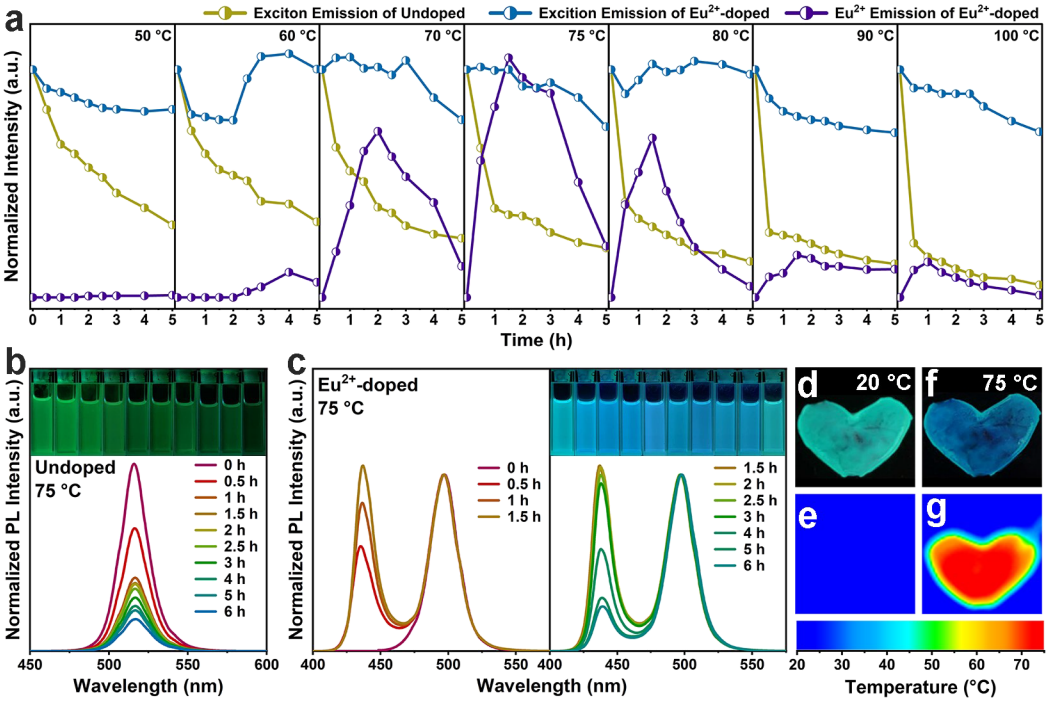

Figure 5. (a) Exciton emission intensity of undoped and Eu^{2+}-doped $CsPbBr_3$ (x = 7.9%) NCs continuously heated at different temperatures (undoped: yellow dotted plot, Eu^{2+}-doped: blue dotted plot) and Eu^{2+} emission intensities (purple dotted line graph): 50, 60, 70, 75, 80, 90, 100 °C with increasing heating time. (b) Normalized PL spectra of undoped $CsPbBr_3$ NCs continuously heated at 75 °C with increasing heating time (excitation at 365 nm). (c) Normalized PL spectra of Eu^{2+}-doped $CsPbBr_3$ (x = 7.9%) NCs continuously heated at 75 °C with increasing heating time (excitation at 365 nm). (d) Photograph of the Eu^{2+}-doped $CsPbBr_3$ NC-based film at room temperature under UV excitation. (e) Thermal image of the Eu^{2+}-doped $CsPbBr_3$ NCs-based film at room temperature. (f) Photograph of the Eu^{2+}-doped $CsPbBr_3$ NC-based film after continuous heating at 75 °C for 48 h under UV excitation. (g) Thermal image of the Eu^{2+}-doped $CsPbBr_3$ NC-based film after continuous heating at 75 °C for 48 h.

When dispersed in dimethylsulfoxide, neither undoped nor Eu^{2+}-doped NCs have emissions. These results indicate that Eu^{2+} doping improves the stability of $CsPbBr_3$ NCs and their resistance to the damage from polar solvents.

In order to uncover whether the improvement of the stability of $CsPbBr_3$ NCs is regularly related to the Eu^{2+} doping ratio, Eu^{2+}-doped $CsPbBr_3$ NCs with different Eu^{2+} doping ratios (x = 0%, x = 1.3%, x = 3.6%, and x = 7.9%) are also selected to measure stability under UV irradiation, corrosive moisture, and polar solvent molecule corrosion. As shown in Figures S8–S10, the improvement of the stability of $CsPbBr_3$ NCs by doping Eu^{2+} is linearly related to the Eu^{2+} doping ratio. Eu^{2+}-doped $CsPbBr_3$ NCs with the highest doping ratio (x = 7.9%) possesses the best stability in all alternative harsh conditions.

With a view to explore the thermal stability of undoped and Eu^{2+}-doped (x = 7.9%) $CsPbBr_3$ NCs, the toluene colloidal solution of the samples are placed in a sand bath and heated continually for several hours. Simultaneously, the samples are heated and tested in air without inert gas protection. As the heating temperature and the heating time increase, the excitonic emission intensity of the undoped $CsPbBr_3$ NCs (yellow line) decreases rapidly during the heating process (Figures 5a and S11); meanwhile, the Eu^{2+}-doped $CsPbBr_3$ NCs have an emission peak at 498 nm and an additional emission peak around 440 nm related to the Eu^{2+}, which can be attributed to the energy transfer of $4f^6 5d^1 \rightarrow 4f^7$ ($5d \rightarrow 4f$). The excitonic emission intensity of Eu^{2+}-doped $CsPbBr_3$ NCs (blue line) remains 70% of the initial intensity after heating for 5 h (Figure S12), although it fluctuates up and down because of unavoidable disruption during heating.

Unexpectedly, the emission intensity ratio of Eu^{2+} to exciton is not constant with the change of heating temperature and time. Therefore, the PL spectra of Eu^{2+}-doped $CsPbBr_3$ are normalized to observe the ratio of Eu^{2+} emission intensity to exciton emission intensity (Figure S13). The ratio of the emission intensity of Eu^{2+} to exciton increases first and then decreases with the increase of heating time. In the temperature range from 50 to 75 °C, the intensity ratio of Eu^{2+} emission to exciton emission shows an increasing trend, while it is opposite in the temperature range from 75 to 100 °C. Taking 75 °C as an example, the intensity of exciton emission from undoped $CsPbBr_3$ NCs decreases rapidly because of the high-temperature damage, as shown in Figure 5b. Differently, the exciton emission intensity of Eu^{2+}-doped $CsPbBr_3$ NCs shows an extremely slow decreasing trend. When the exciton intensity of Eu^{2+}-doped $CsPbBr_3$ NCs is normalized, the Eu^{2+} emission intensity first increases during the first 1.5 h of heating and then decreases after 1.5 h of heating. As shown in Figure 5c, the inset shows the corresponding images of the colloidal solution of luminescent Eu^{2+}-doped $CsPbBr_3$ NCs under UV excitation for different time periods heated at 75 °C, exhibiting the transition of the emitted light from cyan to blue and back to cyan.

The polymethyl methacrylate (PMMA) composite film encapsulated with Eu^{2+}-doped $CsPbBr_3$ (x = 7.9%) NCs is heated at 75 °C in air for investigating whether such a peculiar luminescence phenomenon can only exist in solution. As shown in Figure 5d, under UV excitation, the composite film

https://doi.org/10.1021/jacsau.2c00593
JACS Au 2023, 3, 216–226

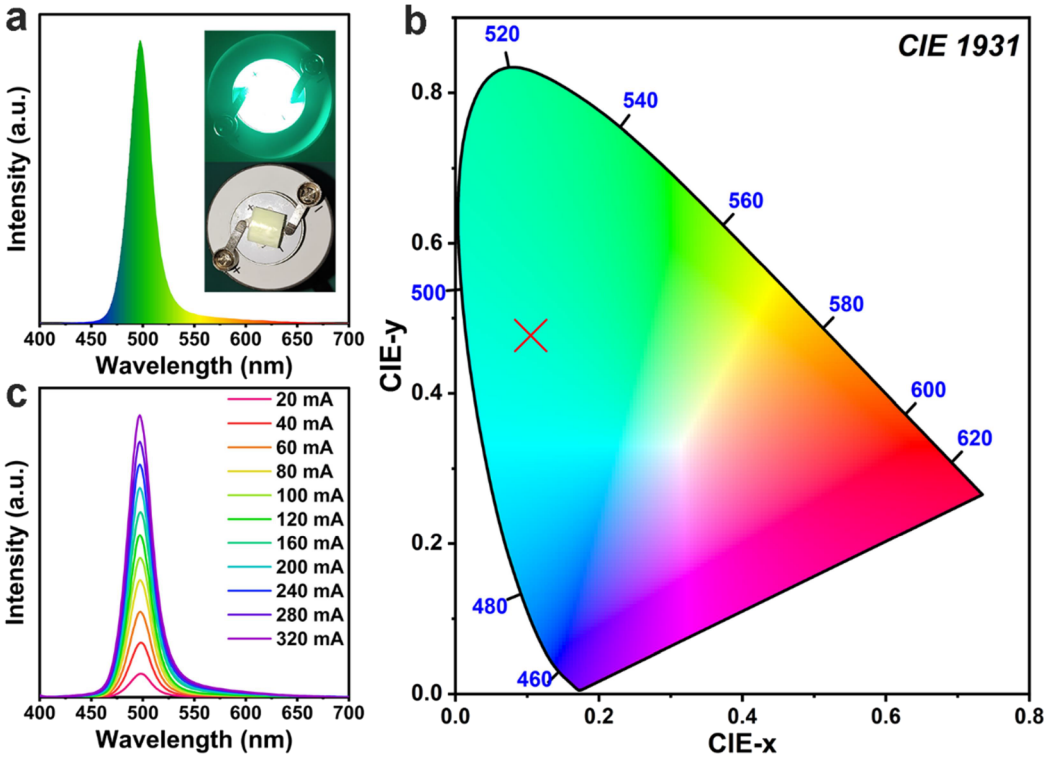

Figure 6. (a) Luminescence spectra of Eu^{2+}-doped $CsPbBr_3$ NC-based LEDs and the inset photograph of an operating LED emitting cyan light at 499 nm. (b) CIE coordinates corresponding to the LED device (red cross). (c) Emission spectra of the LED device at different driving currents.

emits the same cyan-blue light as the Eu^{2+}-doped $CsPbBr_3$ NC colloidal solution before heating, proving that the addition of PMMA has no influence on the luminescence of Eu^{2+}-doped $CsPbBr_3$ NCs. From the thermal image in Figure 5e, the temperature of Eu^{2+}-doped $CsPbBr_3$ NC-based film is generally the same as the surrounding environment before heating. After continuous heating at 75 °C for 48 h, the composite film emits blue light under UV excitation (Figure 5f), which is consistent with the luminescence change produced by the Eu^{2+}-doped $CsPbBr_3$ NC colloidal solution when heated at 75 °C. The temperature of the Eu^{2+}-doped $CsPbBr_3$ NCs-based thin film upon heating is indicated by the thermal image shown in Figure 5g. It can be concluded that the transition from cyan to blue light emission of Eu^{2+}-doped $CsPbBr_3$ NCs under continuous heating at 75 °C is not attributed to the solution effect of toluene.

It has been reported that Eu^{2+} exhibits temperature sensitivity and temperature dependence because of the strong interaction of Eu^{2+} 5d electrons with the local crystal field.[44−46] Moreover, the emission of Eu^{2+} varies with the doping host.[47] Therefore, the energy absorption and transfer of the $CsPbBr_3$ NCs initially induced by continuous heating results in the appearance of the Eu^{2+} emission corresponding to 5d → 4f parity-allowed transitions.[48−50] Based on the reported work, the variation of the Eu^{2+} emission intensity could be relevant to the balance between thermal ionization and recombination of Eu^{2+} 5d-excited state centers with the involvement of electrons trapped at crystal defect levels.[46,48] Then, with the increase of temperature, the increase in the Eu^{2+} emission intensity is likely to be associated with the increase in thermal energy which favors the recombination process.[46] With the further increase of temperature, the decrease of the emission intensity of Eu^{2+} is related to the conventional thermal quenching behavior.[44−46] In addition, increasing the heating time achieves a similar effect as increasing the heating temperature.

The XRD patterns of undoped and Eu^{2+}-doped $CsPbBr_3$ (x = 7.9%) NCs are monitored at several different temperatures (20, 50, 70, 90, and 110 °C) in order to further explore the stability of the crystal structure. By comparing the XRD patterns of undoped $CsPbBr_3$ NCs at different temperatures in Figure S14, it is found that the $CsPbBr_3$ NCs have obvious phase transitions (orthorhombic phase−tetragonal phase) in the temperature ranging from 20 to 110 °C, consistent with the reported temperature-reversible phase transition of $CsPbBr_3$.[51,52] However, the XRD patterns of the Eu^{2+}-doped $CsPbBr_3$ NCs at different temperatures do not show clear differences, indicating that doping Eu^{2+} contributes to the stability of the crystal structure of $CsPbBr_3$ NCs.

Although $CsPb(BrCl)_3$ NCs have been reported to improve the optical properties and stability in relatively mild environments through B-site doping, the enhancement of stability in harsh conditions is rarely reported (Table S4). The stability of $CsPbBr_3$ NCs after Eu^{2+} doping is greatly improved in various harsh conditions, including long-term UV lamp irradiation, aggressive water and polar solvents, and prolonged heating treatment in the air. When it comes to the reasons behind stability improvements, there are several scenarios that deserve being noted here. First, the first-principles calculations of Eu^{2+}-doped $CsPbBr_3$ perovskite have been reported, indicating that the formation energy of doping Eu^{2+} is small, about 0.13 eV per Eu atom, and the Eu^{2+}-doped $CsPbBr_3$ perovskite matrix is energetically stable, where the strain in the system is negligible.[37] Second, the electronegativity of Eu is small compared to that of lead. Previous first-principle calculations uncovered that as lead is more electronegative, electrons are transferred from the doped cation to the adjacent Pb−Br pair.[28] Therefore, the fact of Eu^{2+} partly occupying the Pb^{2+}

https://doi.org/10.1021/jacsau.2c00593
JACS Au 2023, 3, 216−226

site leads to the shortened Pb−Br bond length and the strengthened Pb−Br bond, which is verified by XPS analysis results. Because each of the B-site cations is connected to eight cuboctahedra through $[BX_6]^{4-}$ octahedra, ignoring any possible structural relaxation, reducing the size of one B-site cation reduces the size of the eight cuboctahedrons and voids, thus reducing the rotation or tilt of the $[BX_6]^{4-}$ octahedron.[24] Third, Eu^{2+}-doped $CsPbBr_3$ NCs obtain a higher Goldschmidt tolerance factor, conducive to the stabilization of $CsPbBr_3$.[24] Last but not least, surface passivation of Ln halides also contributes to improving stability by reducing surface defects.[12,25,38,53]

In addition, Eu^{2+}-doped $CsPbCl_3$ was also successfully synthesized, and its PL stability under UV irradiation was improved (Figure S15), which is similar to Eu^{2+}-doped $CsPbBr_3$. Therefore, based on our discovery and previous reported results,[54] doping Eu^{2+} into $CsPbX_3$ NCs results in negligible deformation/strain of the crystal structure and is beneficial to the stability of the system.[23]

The prepared PMMA composite film described above was further deposited on the UV LED and excited by the UV LED chip. The normalized PL spectra of Eu^{2+}-doped $CsPbBr_3$ (x = 7.9%) NC-based LEDs show narrow emission with a peak width at half maximum around 24 nm, as shown in Figure 6a. According to the CIE 1931 standard color matching functions, the emitted green light can be demonstrated by (x, y) chromaticity coordinates (0.1093, 0.4622), as shown in Figure 6b. As shown in Figure 6c, the luminous intensity of this LED increases linearly with current density, which is characteristic of exciton luminescence, and this result excludes the defect luminescence inside the $CsPbBr_3$ NCs after Eu^{2+} doping. Furthermore, Eu^{2+}-doped $CsPbBr_{1.8}Cl_{1.2}$ NCs, that glow bright blue under ultraviolet light, are successfully synthesized. Similar to Eu^{2+}-doped $CsPbBr_3$ NCs, the emission peak of Eu^{2+}-doped $CsPbBr_{1.8}Cl_{1.2}$ NCs is blue-shifted from 480 to 466 nm, and its QY is as high as 91.2% (Figure S16). Eu^{2+}-doped $CsPbBr_{1.8}Cl_{1.2}$ NCs may provide an efficient option for the high EQE and stability of blue halide perovskite LEDs, and these will be investigated in our further study. The above results demonstrate that Eu^{2+} doping improves the stability of $CsPbX_3$ NCs, enriches the optical properties of the material, and further provides a material modification strategy for its applications in many fields such as luminescence and anti-counterfeiting.

3. CONCLUSIONS

In summary, we have successfully introduced Eu^{2+} to replace Pb^{2+} in colloidal $CsPbBr_3$ NCs. The emission spectrum of Eu^{2+}-doped $CsPbBr_3$ NCs can be tuned from green to cyan by controlling the doping concentration of Eu^{2+}. Thanks to the incorporation of Eu^{2+} with negligible strain generated in crystals, the stability of $CsPbBr_3$ NCs is successfully improved in various harsh conditions, including UV irradiation, erosion of moisture, and corrosion of polar solvent molecules. Moreover, compared with undoped $CsPbBr_3$ NCs, the thermal stability of Eu^{2+}-doped $CsPbBr_3$ NCs is greatly enhanced under heating. Meanwhile, the Eu^{2+}-doped $CsPbBr_3$ also exhibits the emissions of Eu^{2+} under prolonged heating. Therefore, doping Eu^{2+} to partially replace Pb^{2+} into all-inorganic $CsPbBr_3$ perovskite NCs is a promising approach to improve their stability under practical harsh environments. Besides, based on the improved stability and quantum yield, Eu^{2+}-doped $CsPbBr_3$ (x = 7.9%) NC-based cyan LED is fabricated, exhibiting narrow exciton emission driven under different current densities. Therefore, the doping of Eu^{2+} and the successful preparation of perovskite cyan LEDs suggest that Ln ion B-site doping is a reliable strategy to optimize perovskites for broader optoelectronic applications.

4. EXPERIMENTAL SECTION

4.1. Preparation of Cs-Oleate

Cs_2CO_3 (0.1628 g), OA (0.5 mL), and ODE (8 mL) were added into a three-necked flask and dried under vacuum at 120 °C for 1 h. Then, the reaction mixture was heated to 150 °C under Ar and kept at this temperature for 0.5 h until Cs_2CO_3 was completely dissolved.

4.2. Synthesis of $CsPbBr_3$ NCs

$PbBr_2$ (0.069 g) and ODE (5 mL) were added to a three-necked flask and dried under vacuum at 120 °C for 0.5 h. Dried OM (0.5 mL) and dried OA (0.5 mL) were injected at 120 °C under Ar. The solution was then heated to 200 °C and maintained for 10 min. Afterward, as-prepared Cs-oleate (0.4 mL) was quickly injected and the reaction mixture was cooled by an ice-water bath after 30 s.

4.3. Synthesis of Eu^{2+}-Doped $CsPbX_3$ NCs

For instance, Eu^{2+}-doped $CsPbBr_3$ (x = 7.2%) NCs were synthesized by adding $EuBr_2$ (0.056 g), thoroughly ground into very fine powder, $PbBr_2$ (0.044 g), and ODE (5 mL) to a three-necked flask and dried under vacuum at 120 °C for 0.5 h to remove H_2O and O_2 molecules. Dried OM (1 mL) and dried OA (0.5 mL) were injected at 120 °C under Ar, whereafter the reaction mixture was put under vacuum and refilled with Ar gas several times at 120 °C for 2 h. The temperature was raised to 200 °C and maintained for 1 h to completely dissolve $PbBr_2$ and $EuBr_2$. Afterward, as-prepared Cs-oleate (0.25 mL) was rapidly injected into the reaction vessel. After 30 s, the reaction mixture was cooled by an ice-water bath. Eu^{2+}-doped $CsPbCl_3$ was synthesized by $EuCl_2$ (0.041 g) and $PbCl_2$ (0.034 g), and Eu^{2+}-doped $CsPbBr_{1.8}Cl_{1.2}$ was synthesized by $EuBr_2$ (0.056 g) and $PbCl_2$ (0.034 g).

4.4. Purification

The crude sample was separated by centrifugation at 15,000 rpm for 10 min to retain the precipitate. Then, in order to remove unreacted components and byproducts, the precipitate was dispersed in toluene and centrifuged at 1000 rpm to remove the precipitate and leave the luminous supernatant. Subsequently, the dispersion was stored in a refrigerator at −4 °C.

4.5. Preparation of PMMA-Eu^{2+}-Doped $CsPbBr_3$ NCs Composite Films

One gram of PMMA was dissolved in toluene with a concentration of 200 mg mL^{-1} at 40 °C. Ten milliliters of NCs were added into the PMMA solution and stirred vigorously for 1 h. In order to prepare a PMMA-Eu^{2+}-doped $CsPbBr_3$ NCs film, the mixed solution was cast onto the surface of a 2 cm × 2 cm quartz substrate and the film was dried under vacuum overnight.

■ ASSOCIATED CONTENT

Supporting Information

The Supporting Information is available free of charge at https://pubs.acs.org/doi/10.1021/jacsau.2c00593.

Experimental details; characterization data; and additional data (PDF)

■ AUTHOR INFORMATION

Corresponding Authors

Zongyou Yin − *Research School of Chemistry, Australian National University, Canberra, ACT 2601, Australia;* orcid.org/0000-0002-0800-4490; Email: zongyou.yin@anu.edu.au

https://doi.org/10.1021/jacsau.2c00593
JACS Au 2023, 3, 216−226

Yaping Du − *Tianjin Key Lab for Rare Earth Materials and Applications, Center for Rare Earth and Inorganic Functional Materials, Smart Sensing Interdisciplinary Science Center, School of Materials Science and Engineering & National Institute for Advanced Materials, Nankai University, Tianjin 300350, P.R. China*; orcid.org/0000-0002-9937-2087; Email: ypdu@nankai.edu.cn

Authors

Mengdie Jin − *Tianjin Key Lab for Rare Earth Materials and Applications, Center for Rare Earth and Inorganic Functional Materials, Smart Sensing Interdisciplinary Science Center, School of Materials Science and Engineering & National Institute for Advanced Materials, Nankai University, Tianjin 300350, P.R. China*

Zhichao Zeng − *Tianjin Key Lab for Rare Earth Materials and Applications, Center for Rare Earth and Inorganic Functional Materials, Smart Sensing Interdisciplinary Science Center, School of Materials Science and Engineering & National Institute for Advanced Materials, Nankai University, Tianjin 300350, P.R. China*

Hao Fu − *College of Chemistry, Nankai University, Tianjin 300071, P.R. China*

Siyuan Wang − *Tianjin Key Lab for Rare Earth Materials and Applications, Center for Rare Earth and Inorganic Functional Materials, Smart Sensing Interdisciplinary Science Center, School of Materials Science and Engineering & National Institute for Advanced Materials, Nankai University, Tianjin 300350, P.R. China*

Xinyun Zhai − *Tianjin Key Lab for Rare Earth Materials and Applications, Center for Rare Earth and Inorganic Functional Materials, Smart Sensing Interdisciplinary Science Center, School of Materials Science and Engineering & National Institute for Advanced Materials, Nankai University, Tianjin 300350, P.R. China*

Qian Zhang − *State Key Laboratory of Eco-Hydraulics in Northwest Arid Region, Department of Applied Chemistry, Xi'an University of Technology, Xi'an 710048, P.R. China*

Complete contact information is available at: https://pubs.acs.org/10.1021/jacsau.2c00593

Author Contributions

The manuscript was written through contributions of all authors. CRediT: **Mengdie Jin** data curation, investigation, writing-original draft; **Zhichao Zeng** data curation, formal analysis, investigation, writing-review & editing; **Hao Fu** formal analysis, investigation, writing-review & editing; **Siyuan Wang** formal analysis, investigation, writing-review & editing; **Zongyou Yin** investigation, supervision, writing-review & editing; **Xinyun Zhai** formal analysis, investigation, writing-review & editing; **Qian Zhang** investigation, resources, supervision, writing-review & editing; **Yaping Du** conceptualization, formal analysis, funding acquisition, resources, supervision, writing-review & editing.

Notes

The authors declare no competing financial interest.

■ ACKNOWLEDGMENTS

We gratefully acknowledge the support from the National Natural Science Foundation of China (21971117), the 111 Project (B18030) from China, the Beijing−Tianjin−Hebei Collaborative Innovation Project (19YFSLQY00030), the Outstanding Youth Project of Tianjin Natural Science Foundation (20JCJQJC00130), the Key Project of Tianjin Natural Science Foundation (20JCZDJC00650), the Open Foundation of Guangxi Key Laboratory of Processing for Non-ferrous Metals and Featured Materials (Grant No. 2022GXY-SOF07), the Functional Research Funds for the Central Universities, Nankai University (ZB19500202), Tianjin "131" Innovative Talent Team Construction Project, Tianjin Key Laboratory for Rare Earth Materials and Applications (ZB19500202), and the Haihe Laboratory of Sustainable Chemical Transformations for financial support.

■ REFERENCES

(1) Protesescu, L.; Yakunin, S.; Bodnarchuk, M. I.; Krieg, F.; Caputo, R.; Hendon, C. H.; Yang, R. X.; Walsh, A.; Kovalenko, M. V. Nanocrystals of Cesium Lead Halide Perovskites ($CsPbX_3$, X = Cl, Br, and I): Novel Optoelectronic Materials Showing Bright Emission with Wide Color Gamut. *Nano Lett.* **2015**, *15*, 3692−3696.

(2) Nedelcu, G.; Protesescu, L.; Yakunin, S.; Bodnarchuk, M. I.; Grotevent, M. J.; Kovalenko, M. V. Fast Anion-Exchange in Highly Luminescent Nanocrystals of Cesium Lead Halide Perovskites ($CsPbX_3$, X = Cl, Br, I). *Nano Lett.* **2015**, *15*, 5635−5640.

(3) Zhang, X.; Lin, H.; Huang, H.; Reckmeier, C.; Zhang, Y.; Choy, W. C.; Rogach, A. L. Enhancing the Brightness of Cesium Lead Halide Perovskite Nanocrystal Based Green Light-Emitting Devices through the Interface Engineering with Perfluorinated Ionomer. *Nano Lett.* **2016**, *16*, 1415−1420.

(4) Pan, J.; Shang, Y.; Yin, J.; De Bastiani, M.; Peng, W.; Dursun, I.; Sinatra, L.; El-Zohry, A. M.; Hedhili, M. N.; Emwas, A. H.; Mohammed, O. F.; Ning, Z.; Bakr, O. M. Bidentate Ligand-Passivated $CsPbI_3$ Perovskite Nanocrystals for Stable Near-Unity Photoluminescence Quantum Yield and Efficient Red Light-Emitting Diodes. *J. Am. Chem. Soc.* **2018**, *140*, 562−565.

(5) Altintas, Y.; Torun, I.; Yazici, A. F.; Beskazak, E.; Erdem, T.; Serdar Onses, M.; Mutlugun, E. Multiplexed Patterning of Cesium Lead Halide Perovskite Nanocrystals by Additive Jet Printing for Efficient White Light Generation. *Chem. Eng. J.* **2020**, *380*, No. 122493.

(6) Lu, M.; Guo, J.; Sun, S.; Lu, P.; Zhang, X.; Shi, Z.; Yu, W. W.; Zhang, Y. Surface Ligand Engineering-Assisted $CsPbI_3$ Quantum Dots Enable Bright and Efficient Red Light-Emitting Diodes with a Top-Emitting Structure. *Chem. Eng. J.* **2021**, *404*, No. 126563.

(7) Xu, J.; Huang, W.; Li, P.; Onken, D. R.; Dun, C.; Guo, Y.; Ucer, K. B.; Lu, C.; Wang, H.; Geyer, S. M.; Williams, R. T.; Carroll, D. L. Imbedded Nanocrystals of $CsPbBr_3$ in Cs_4PbBr_6: Kinetics, Enhanced Oscillator Strength, and Application in Light-Emitting Diodes. *Adv. Mater.* **2017**, *29*, No. 1703703.

(8) Lu, P.; Lu, M.; Wang, H.; Sui, N.; Shi, Z.; Yu, W. W.; Zhang, Y. Metal Halide Perovskite Nanocrystals and Their Applications in Optoelectronic Devices. *InfoMat* **2019**, *1*, 430−459.

(9) Gao, Y.; Wu, Y.; Lu, H.; Chen, C.; Liu, Y.; Bai, X.; Yang, L.; Yu, W.; Dai, Q.; Zhang, Y. $CsPbBr_3$ Perovskite Nanoparticles as Additive for Environmentally Stable Perovskite Solar Cells with 20.46% Efficiency. *Nano Energy* **2019**, *59*, 517−526.

(10) Gao, Y.; Wu, Y.; Liu, Y.; Lu, M.; Yang, L.; Wang, Y.; Yu, W. W.; Bai, X.; Zhang, Y.; Dai, Q. Interface and Grain Boundary Passivation for Efficient and Stable Perovskite Solar Cells: The Effect of Terminal Groups in Hydrophobic Fused Benzothiadiazole-Based Qrganic Semiconductors. *Nano Horiz.* **2020**, *5*, 1574−1585.

(11) Wang, M.; Wang, W.; Ma, B.; Shen, W.; Liu, L.; Cao, K.; Chen, S.; Huang, W. Lead-Free Perovskite Materials for Solar Cells. *Nano-Micro Lett.* **2021**, *13*, 62.

(12) Zhou, D.; Sun, R.; Xu, W.; Ding, N.; Li, D.; Chen, X.; Pan, G.; Bai, X.; Song, H. Impact of Host Composition, Codoping, or Tridoping on Quantum-Cutting Emission of Ytterbium in Halide Perovskite Quantum Dots and Solar Cell Applications. *Nano Lett.* **2019**, *19*, 6904−6913.

(13) Pan, J.; Sarmah, S. P.; Murali, B.; Dursun, I.; Peng, W.; Parida, M. R.; Liu, J.; Sinatra, L.; Alyami, N.; Zhao, C.; Alarousu, E.; Ng, T. K.; Ooi, B. S.; Bakr, O. M.; Mohammed, O. F. Air-Stable Surface-Passivated Perovskite Quantum Dots for Ultra-Robust, Single- and Two-Photon-Induced Amplified Spontaneous Emission. *J. Phys. Chem. Lett.* **2015**, *6*, 5027−5033.
(14) Zhang, Y.; Sun, R.; Ou, X.; Fu, K.; Chen, Q.; Ding, Y.; Xu, L. J.; Liu, L.; Han, Y.; Malko, A. V.; Liu, X.; Yang, H.; Bakr, O. M.; Liu, H.; Mohammed, O. F. Metal Halide Perovskite Nanosheet for X-ray High-Resolution Scintillation Imaging Screens. *ACS Nano* **2019**, *13*, 2520−2525.
(15) Chen, Q.; Wu, J.; Ou, X.; Huang, B.; Almutlaq, J.; Zhumekenov, A. A.; Guan, X.; Han, S.; Liang, L.; Yi, Z.; Li, J.; Xie, X.; Wang, Y.; Li, Y.; Fan, D.; Teh, D. B. L.; All, A. H.; Mohammed, O. F.; Bakr, O. M.; Wu, T.; Bettinelli, M.; Yang, H.; Huang, W.; Liu, X. All-inorganic Perovskite Nanocrystal Scintillators. *Nature* **2018**, *561*, 88−93.
(16) Song, J.; Xu, L.; Li, J.; Xue, J.; Dong, Y.; Li, X.; Zeng, H. Monolayer and Few-Layer All-Inorganic Perovskites as a New Family of Two-Dimensional Semiconductors for Printable Optoelectronic Devices. *Adv. Mater.* **2016**, *28*, 4861−4869.
(17) Almeida, G.; Goldoni, L.; Akkerman, Q.; Dang, Z.; Khan, A. H.; Marras, S.; Moreels, I.; Manna, L. Role of Acid-Base Equilibria in the Size, Shape, and Phase Control of Cesium Lead Bromide Nanocrystals. *ACS Nano* **2018**, *12*, 1704−1711.
(18) Shamsi, J.; Dang, Z.; Bianchini, P.; Canale, C.; Stasio, F. D.; Brescia, R.; Prato, M.; Manna, L. Colloidal Synthesis of Quantum Confined Single Crystal $CsPbBr_3$ Nanosheets with Lateral Size Control Up to the Micrometer Range. *J. Am. Chem. Soc.* **2016**, *138*, 7240−7243.
(19) Imran, M.; Di Stasio, F.; Dang, Z.; Canale, C.; Khan, A. H.; Shamsi, J.; Brescia, R.; Prato, M.; Manna, L. Colloidal Synthesis of Strongly Fluorescent $CsPbBr_3$ Nanowires with Width Tunable down to the Quantum Confinement Regime. *Chem. Mater.* **2016**, *28*, 6450−6454.
(20) Zhang, D.; Yang, Y.; Bekenstein, Y.; Yu, Y.; Gibson, N. A.; Wong, A. B.; Eaton, S. W.; Kornienko, N.; Kong, Q.; Lai, M.; Alivisatos, A. P.; Leone, S. R.; Yang, P. Synthesis of Composition Tunable and Highly Luminescent Cesium Lead Halide Nanowires through Anion-Exchange Reactions. *J. Am. Chem. Soc.* **2016**, *138*, 7236−7239.
(21) Shamsi, J.; Urban, A. S.; Imran, M.; De Trizio, L.; Manna, L. Metal Halide Perovskite Nanocrystals: Synthesis, Post-Synthesis Modifications, and Their Optical Properties. *Chem. Rev.* **2019**, *119*, 3296−3348.
(22) He, L.; Meng, J.; Feng, J.; Liu, X.; Zhang, H. Unveiling the Mechanism of Rare Earth Doping to Optimize the Optical Performance of the $CsPbBr_3$ Perovskite. *Inorg. Chem. Front.* **2020**, *7*, 4669−4676.
(23) Mir, W. J.; Sheikh, T.; Arfin, H.; Xia, Z.; Nag, A. Lanthanide Doping in Metal Halide Perovskite Nanocrystals: Spectral Shifting Quantum Cutting and Optoelectronic Applications. *NPG Asia Mater.* **2020**, *12*, 9.
(24) Swarnkar, A.; Mir, W. J.; Nag, A. Can B-Site Doping or Alloying Improve Thermal- and Phase-Stability of All-Inorganic $CsPbX_3$ (X = Cl, Br, I) Perovskites? *ACS Energy Lett.* **2018**, *3*, 286−289.
(25) Pan, G.; Bai, X.; Yang, D.; Chen, X.; Jing, P.; Qu, S.; Zhang, L.; Zhou, D.; Zhu, J.; Xu, W.; Dong, B.; Song, H. Doping Lanthanide into Perovskite Nanocrystals: Highly Improved and Expanded Optical Properties. *Nano Lett.* **2017**, *17*, 8005−8011.
(26) Zhao, H.; Xia, J.; Yin, D.; Luo, M.; Yan, C.; Du, Y. Rare Earth incorporated Electrode Materials for Advanced Energy Storage. *Coord. Chem. Rev.* **2019**, *390*, 32−49.
(27) Yao, J. S.; Ge, J.; Han, B. N.; Wang, K. H.; Yao, H. B.; Yu, H. L.; Li, J. H.; Zhu, B. S.; Song, J. Z.; Chen, C.; Zhang, Q.; Zeng, H. B.; Luo, Y.; Yu, S. H. Ce^{3+}-Doping to Modulate Photoluminescence Kinetics for Efficient $CsPbBr_3$ Nanocrystals Based Light-Emitting Diodes. *J. Am. Chem. Soc.* **2018**, *140*, 3626−3634.
(28) Xie, Y.; Peng, B.; Bravic, I.; Yu, Y.; Dong, Y.; Liang, R.; Ou, Q.; Monserrat, B.; Zhang, S. Highly Efficient Blue-Emitting $CsPbBr_3$ Perovskite Nanocrystals through Neodymium Doping. *Adv. Sci.* **2020**, *7*, No. 2001698.
(29) Li, Q.; Liu, Y.; Chen, P.; Hou, J.; Sun, Y.; Zhao, G.; Zhang, N.; Zou, J.; Xu, J.; Fang, Y.; Dai, N. Excitonic Luminescence Engineering in Tervalent-Europium-Doped Cesium Lead Halide Perovskite Nanocrystals and Their Temperature-Dependent Energy Transfer Emission Properties. *J. Phys. Chem. C* **2018**, *122*, 29044−29050.
(30) Chen, Y.-C.; Chou, H.-L.; Lin, J.-C.; Lee, Y.-C.; Pao, C.-W.; Chen, J.-L.; Chang, C.-C.; Chi, R.-Y.; Kuo, T.-R.; Lu, C.-W.; Wang, D.-Y. Enhanced Luminescence and Stability of Cesium Lead Halide Perovskite $CsPbX_3$ Nanocrystals by Cu^{2+}-Assisted Anion Exchange Reactions. *J. Phys. Chem. C* **2019**, *123*, 2353−2360.
(31) Yong, Z.-J.; Guo, S.-Q.; Ma, J.-P.; Zhang, J.-Y.; Li, Z.-Y.; Chen, Y.-M.; Zhang, B.-B.; Zhou, Y.; Shu, J.; Gu, J.-L.; Zheng, L.-R.; Bakr, O. M.; Sun, H.-T. Doping-Enhanced Short-Range Order of Perovskite Nanocrystals for Near-Unity Violet Luminescence Quantum Yield. *J. Am. Chem. Soc.* **2018**, *140*, 9942−9951.
(32) Zhang, Y.; Jie, W.; Chen, P.; Liu, W.; Hao, J. Ferroelectric and Piezoelectric Effects on the Optical Process in Advanced Materials and Devices. *Adv. Mater.* **2018**, *30*, No. 1707007.
(33) An, R.; Zhao, H.; Hu, H. M.; Wang, X.; Yang, M. L.; Xue, G. Synthesis, Structure, White-Light Emission, and Temperature Recognition Properties of Eu/Tb Mixed Coordination Polymers. *Inorg. Chem.* **2016**, *55*, 871−876.
(34) Xiang, W.; Wang, Z.; Kubicki, D. J.; Tress, W.; Luo, J.; Prochowicz, D.; Akin, S.; Emsley, L.; Zhou, J.; Dietler, G.; Grätzel, M.; Hagfeldt, A. Europium-Doped $CsPbI_2Br$ for Stable and Highly Efficient Inorganic Perovskite Solar Cells. *Joule* **2019**, *3*, 205−214.
(35) Cheng, Y.; Shen, C.; Shen, L.; Xiang, W.; Liang, X. Tb^{3+}, Eu^{3+} Co-doped $CsPbBr_3$ QDs Glass with Highly Stable and Luminous Adjustable for White LEDs. *ACS Appl. Mater. Interfaces* **2018**, *10*, 21434−21444.
(36) Wu, X.; Li, H.; Wang, K.; Sun, X.; Wang, L. $CH_3NH_3Pb_{1-x}Eu_xI_3$ Mixed Halide Perovskite for Hybrid Solar Cells: The Impact of Divalent Europium Doping on Efficiency and Stability. *RSC Adv.* **2018**, *8*, 11095−11101.
(37) Bala, A.; Kumar, V. Stability of the Eu^{2+} Dopant in $CsPbBr_3$ Perovskites: A First-Principles Study. *J. Phys. Chem. C* **2019**, *123*, 6965−6969.
(38) Dang, Z.; Shamsi, J.; Palazon, F.; Imran, M.; Akkerman, Q. A.; Park, S.; Bertoni, G.; Prato, M.; Brescia, R.; Manna, L. In Situ Transmission Electron Microscopy Study of Electron Beam-Induced Transformations in Colloidal Cesium Lead Halide Perovskite Nanocrystals. *ACS Nano* **2017**, *11*, 2124−2132.
(39) Glaser, P.; Stewart, O., Jr.; Atif, R.; Asuigui, D. R. C.; Swanson, J.; Biacchi, A. J.; Hight Walker, A. R.; Morrison, G.; Zur Loye, H. C.; Stoll, S. L. Synthesis of Mixed-Valent Lanthanide Sulfide Nanoparticles. *Angew. Chem., Int. Ed.* **2021**, *60*, 23134−23141.
(40) Jiang, W.; Bian, Z.; Hong, C.; Huang, C. A Mild Liquid Reduction Route Toward Uniform Blue-Emitting $EuCl_2$ Nanoprisms and Nanorods. *Inorg. Chem.* **2011**, *50*, 6862−6864.
(41) Zhao, F.; Sun, H. L.; Su, G.; Gao, S. Synthesis and Size-Dependent Magnetic Properties of Monodisperse EuS Nanocrystals. *Small* **2006**, *2*, 244−248.
(42) Wang, C.; Zhang, D.; Xu, L.; Jiang, Y.; Dong, F.; Yang, B.; Yu, K.; Lin, Q. A Simple Reducing Approach Using Amine to Give Dual Functional EuSe Nanocrystals and Morphological Tuning. *Angew. Chem., Int. Ed.* **2011**, *50*, 7587−7591.
(43) Makula, P.; Pacia, M.; Macyk, W. How to Correctly Determine the Band Gap Energy of Modified Semiconductor Photocatalysts Based on UV-Vis Spectra. *J. Phys. Chem. Lett.* **2018**, *9*, 6814−6817.
(44) Denault, K. A.; Brgoch, J.; Gaultois, M. W.; Mikhailovsky, A.; Petry, R.; Winkler, H.; DenBaars, S. P.; Seshadri, R. Consequences of Optimal Bond Valence on Structural Rigidity and Improved Luminescence Properties in $Sr_xBa_{2-x}SiO_4:Eu^{2+}$ Orthosilicate Phosphors. *Chem. Mater.* **2014**, *26*, 2275−2282.

https://doi.org/10.1021/jacsau.2c00593
JACS Au 2023, 3, 216−226

(45) Wagatha, P.; Weiler, V.; Schmidt, P. J.; Schnick, W. Tailoring Emission Characteristics: Narrow-Band Red Luminescence from SLA to $CaBa[Li_2Al_6N_8]:Eu^{2+}$. *Chem. Mater.* **2018**, *30*, 7885−7891.
(46) Qiao, J.; Ning, L.; Molokeev, M. S.; Chuang, Y. C.; Liu, Q.; Xia, Z. Eu^{2+} Site Preferences in the Mixed Cation $K_2BaCa(PO_4)_2$ and Thermally Stable Luminescence. *J. Am. Chem. Soc.* **2018**, *140*, 9730−9736.
(47) Lefevre, G.; Herfurth, A.; Kohlmann, H.; Sayede, A.; Wylezich, T.; Welinski, S.; Duarte Vaz, P.; Parker, S. F.; Blach, J. F.; Goldner, P.; Kunkel, N. Electron−Phonon Coupling in Luminescent Europium-Doped Hydride Perovskites Studied by Luminescence Spectroscopy, Inelastic Neutron Scattering, and First-Principles Calculations. *J. Phys. Chem. C* **2018**, *122*, 10501−10509.
(48) Shi, R.; Ning, L.; Huang, Y.; Tao, Y.; Zheng, L.; Li, Z.; Liang, H. $Li_4SrCa(SiO_4)_2:Eu^{2+}$: A Potential Temperature Sensor with Unique Optical Thermometric Properties. *ACS Appl. Mater. Interfaces* **2019**, *11*, 9691−9695.
(49) Xia, Z.; Ma, C.; Molokeev, M. S.; Liu, Q.; Rickert, K.; Poeppelmeier, K. R. Chemical Unit Cosubstitution and Tuning of Photoluminescence in the $Ca_2(Al_{1-x}Mg_x)(Al_{1-x}Si_{1+x})O_7:Eu^{2+}$ Phosphor. *J. Am. Chem. Soc.* **2015**, *137*, 12494−12497.
(50) Takeda, T.; Hirosaki, N.; Funahshi, S.; Xie, R.-J. Narrow-Band Green-Emitting Phosphor $Ba_2LiSi_7AlN_{12}:Eu^{2+}$ with High Thermal Stability Discovered by a Single Particle Diagnosis Approach. *Chem. Mater.* **2015**, *27*, 5892−5898.
(51) Malyshkin, D.; Sereda, V.; Ivanov, I.; Mazurin, M.; Sednev-Lugovets, A.; Tsvetkov, D.; Zuev, A. New Phase Transition in $CsPbBr_3$. *Mater. Lett.* **2020**, *278*, No. 128458.
(52) Cottingham, P.; Brutchey, R. L. Depressed Phase Transitions and Thermally Persistent Local Distortions in $CsPbBr_3$ Quantum Dots. *Chem. Mater.* **2018**, *30*, 6711−6716.
(53) Sun, R.; Lu, P.; Zhou, D.; Xu, W.; Ding, N.; Shao, H.; Zhang, Y.; Li, D.; Wang, N.; Zhuang, X.; Dong, B.; Bai, X.; Song, H. Samarium-Doped Metal Halide Perovskite Nanocrystals for Single-Component Electroluminescent White Light-Emitting Diodes. *ACS Energy Lett.* **2020**, *5*, 2131−2139.
(54) Jena, A. K.; Kulkarni, A.; Sanehira, Y.; Ikegami, M.; Miyasaka, T. Stabilization of α-$CsPbI_3$ in Ambient Room Temperature Conditions by Incorporating Eu into $CsPbI_3$. *Chem. Mater.* **2018**, *30*, 6668−6674.

https://doi.org/10.1021/jacsau.2c00593
JACS Au 2023, 3, 216−226